

Crystal Structural Framework of Lithium Super-Ionic Conductors

Xingfeng He, Qiang Bai, Yunsheng Liu, Adelaide M. Nolan, Chen Ling, and Yifei Mo*

As technologically important materials for solid-state batteries, Li super-ionic conductors are a class of materials exhibiting exceptionally high ionic conductivity at room temperature. These materials have unique crystal structural frameworks hosting a highly conductive Li sublattice. However, it is not understood why certain crystal structures of the super-ionic conductors lead to high conductivity in the Li sublattice. In this study, using topological analysis and *ab initio* molecular dynamics simulations, the crystal structures of all Li-conducting oxides and sulfides are studied systematically and the key features pertaining to fast-ion conduction are quantified. In particular, a unique feature of enlarged Li sites caused by large local spaces in the crystal structural framework is identified, promoting fast conduction in the Li-ion sublattice. Based on these quantified features, the high-throughput screening identifies many new structures as fast Li-ion conductors, which are further confirmed by *ab initio* molecular dynamics simulations. This study provides new insights and a systematic quantitative understanding of the crystal structural frameworks of fast ion-conductor materials and motivates future experimental and computational studies on new fast-ion conductors.

replacement of liquid electrolyte and has the potential to achieve improved safety, higher energy density, and longer cycle life than current commercial lithium-ion batteries with liquid electrolytes.^[17] Despite significant research efforts, only a few Li SIC materials exhibit an ionic conductivity of $>10^{-3}$ S cm⁻¹ at room temperature, and some Li SICs suffer from limited stability, poor interfacial compatibility, or high cost in processing and manufacturing.^[6,7,18] A strong need exists for fundamental understanding of these SIC materials in order to design and discover new Li SIC materials.

A Li-ion conductor material is comprised of a mobile Li-ion sublattice hosted in a crystal structural framework of immobile polyanion groups. The empty space in between these polyanion groups hosts Li ions as Li sites and forms interconnected channels. Li ions migrate among the sites through these channels,

1. Introduction

Fast ionic conductors are a critical component of many electrochemical devices, such as batteries, fuel cells, sensors, and electrochemical membranes.^[1–5] Lithium super-ionic conductors (SICs) are a unique class of materials exhibiting high Li ionic conductivity of $>10^{-3}$ S cm⁻¹ at room temperature (RT).^[6–11] Currently known lithium SICs, including Li₁₀GeP₂S₁₂ (LGPS),^[12] garnet Li₇La₃Zr₂O₁₂ (LLZO),^[13,14] and NASICON Li_{1.3}Al_{0.3}Ti_{1.7}(PO₄)₃ (LATP),^[15,16] exhibit comparable conductivities to those of commercial liquid electrolytes. An all-solid-state battery uses Li SICs as an solid electrolyte in

contributing to overall ionic transport. Well-known crystal structural frameworks of SICs include NASICON structure of LiM₂(PO₄)₃ (M = Ge, Ti, Sn, Hf, Zr) compositions,^[19] garnet structure of Li_xLa₃M₂O₁₂ (5 ≤ x ≤ 7, M = Nb, Ta, Sb, Zr, Sn) compositions,^[20] and LGPS-type structure of Li_{10+x}M_{1+x}P_{2-x}S₁₂ (0 ≤ x ≤ 1, M = Si, Ge, Sn) compositions.^[21] Recent studies have demonstrated that the crystal structural framework determines Li sites, migration pathways, and the energy landscape, and particular crystal structural frameworks are optimal for low energy barrier Li ion migration.^[10,22,23] For example, the crystal structural framework with a body-centered cubic (bcc) anion sublattice, such as found in LGPS and Li₇P₃S₁₁, has been shown to have an energy landscape with the lowest barrier compared to other anion sublattices, such as in face-centered cubic and hexagonal close packed sublattices.^[10] However, some SICs with crystal structural frameworks of non-bcc anion sublattices, such as lithium garnet (e.g., LLZO) and lithium NASICON (e.g., LATP), also exhibit high Li⁺ conductivities as high as $\approx 10^{-3}$ S cm⁻¹ at RT. It remains an open question as to what features of these crystal structure frameworks enable super-ionic conduction.

Due to their unique crystal structural frameworks, SIC materials have highly mobile Li-ion sublattices, which are drastically different from those in typical solids (Figure 1). The disordered Li sublattice of SICs facilitates the transport of a large number of Li ions and yields high ionic conductivity. In the disordered Li sublattice, the Li-ion diffusion mechanism is also distinctive

X. He, Q. Bai, Y. Liu, A. M. Nolan, Prof. Y. Mo
Department of Materials Science and Engineering
University of Maryland
College Park, MD 20742, USA
E-mail: yfmo@umd.edu

Dr. C. Ling
Toyota Research Institute of North America
Ann Arbor, MI 48105, USA

Prof. Y. Mo
Maryland Energy Innovation Institute
University of Maryland
College Park, MD 20742, USA

 The ORCID identification number(s) for the author(s) of this article can be found under <https://doi.org/10.1002/aenm.201902078>.

DOI: 10.1002/aenm.201902078

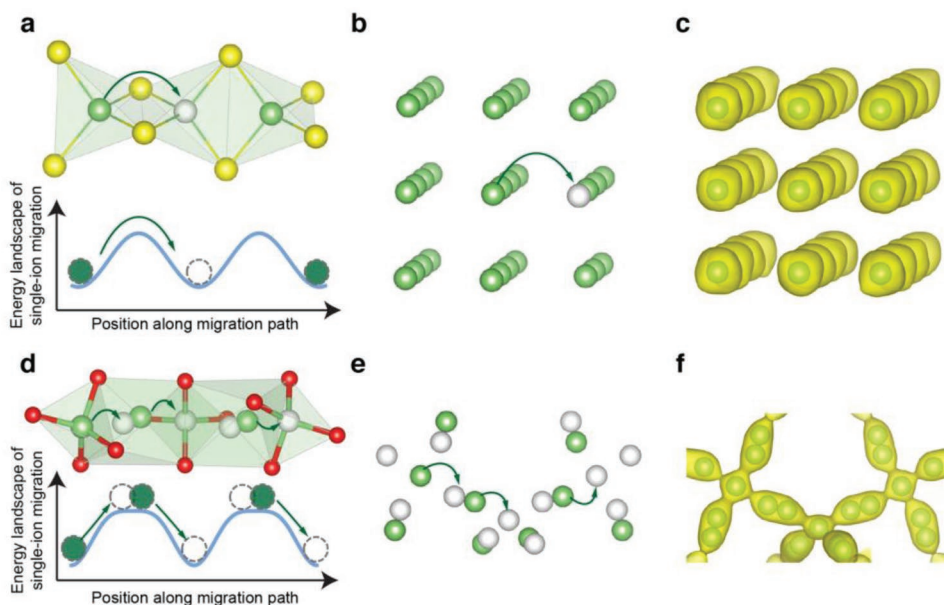


Figure 1. Comparison of Li sublattice and Li⁺ diffusion mechanism in a–c) typical non-SIC solids, e.g., Li₂S versus d–f) an SIC, e.g., garnet LLZO. a,d) Schematic illustration of Li⁺ diffusion pathway in the crystal structural framework (upper) and the energy landscape for Li⁺ migration (lower). b,e) Li sublattice and Li⁺ diffusion mechanism of isolated, individual Li⁺ hopping in typical solids versus concerted migration in an SIC. c,f) Li⁺ probability density from AIMD simulations describing the positional distribution of Li ions.

(Figure 1d–f). Compared to isolated, individual Li⁺ hopping in typical solids (Figure 1a–c), the concerted migration of multiple Li ions exhibits a lower migration energy barrier and is demonstrated as a key diffusion mechanism in SICs^[24–26] (Figure 1d–f). The energetics of the Li-ion sublattice are greatly affected by the strong Coulombic interactions among Li ions in addition to the interactions with the crystal structural framework. For example, as shown by computational studies of lithium garnet, the Li sublattice exhibits disordering at certain Li concentrations as a result of the geometrical frustration.^[27–29] In addition, the Li garnet and other SICs have partially occupied, disordered Li sites within a short distance of <2 Å, which corresponds to a continuous large volume of Li⁺ probability density as revealed by atomistic modeling (Figure 1f).^[10,24] Since the crystal structural framework determines the Li sites and energy landscape, a key question is what crystal structural framework can provide these unique Li sublattices of SICs.

While high-throughput screenings of crystal structural frameworks were conducted,^[30–32] a number of fundamental questions regarding the quantitative features of crystal structural frameworks have not been answered. Among well-known SICs, such as LGPS, garnet, and NASICON, shared structural features among these crystal structural frameworks are not obvious and are yet to be quantified.^[23] Quantitative description and analysis of crystal structural frameworks are needed for identifying the common features in these new SICs. For example, while the bottleneck size of the diffusion channel within a crystal structural framework is known to be critical for ion migration, the optimal values of the bottleneck size for Li⁺ migration have yet to be identified. A short distance between Li sites is hypothesized to facilitate Li migrations, but is yet to be quantitatively confirmed.^[10,22,23] Moreover, it is still not clear

what features of the crystal structural frameworks of SICs can provide a disordered Li sublattice. Therefore, quantitative analyses of crystal structure framework are needed for identifying common features of SICs and for guiding the future discovery of SICs.

In this study, we performed a systematic analysis of the crystal structures of SICs and revealed their unique key features using ab initio molecular dynamics (AIMD) simulations and topological analyses. We identified that SICs have enlarged Li sites given by large local space in the crystal structural framework and that these sites are associated with significant positional disordering of Li ions, which promotes fast ion diffusion (Section 2.1 and 2.2). We systematically analyzed the crystal structural frameworks of all Li-containing oxides and sulfides in the Inorganic Crystal Structure Database (ICSD). From these analyses, we quantified multiple shared features of the crystal structural frameworks of known SICs (Section 2.3). On the basis of these quantified features, we performed high-throughput screening among all known lithium-containing oxide and sulfide compounds for identifying fast ion conductors (Section 2.4). Our high-throughput screening uncovered all known SICs, which confirmed the validity of our approach and quantitative features, and discovered many crystal structural frameworks that have the potential to be fast ion conductors. Using density functional theory (DFT) computations with AIMD simulations (Section 2.5), we studied these newly identified crystal structural frameworks and confirmed 15 structures with appropriate substitution levels are fast ionic conductors with extrapolated Li⁺ conductivities greater than 0.1 mS cm⁻¹ at 300 K. Our study revealed the key features of crystal structural frameworks of SICs and provided guidance for future discovery of fast ion-conducting materials.

2. Results

2.1. Unique Li Site in SICs

We first highlight distinctive features of SICs that are absent in non-SIC materials. The SICs exhibit a disordered Li sublattice, which is critical to achieve high ionic conductivity. In addition to the partial occupancy disordering of the Li sublattice, i.e., disordering with a large number of Li^+ configurations in the Li sublattice, SICs also exhibit positional disordering on some Li sites, where Li^+ moves over a spread of closely spaced positions within a short period of time. Here we found this positional disordering often happens on sites that we refer to as “enlarged Li sites,” which have a large local space suitable for Li^+ occupation at multiple positions as shown by topological

analyses (Experimental Section). The positional disordering on these enlarged sites is reflected by the instantaneous Li positions and Li^+ probability density from AIMD simulations, which is also consistent with the Li sites determined from experimentally observed ion nuclear density.

The positional disordering of Li ion on the enlarged Li site is confirmed by the real-time positions of Li ions in AIMD simulations. As observed in AIMD simulations, Li ions move rapidly over a spread of locations within the enlarged site during a fraction of picosecond. This rapid movement of Li ions is under the typical vibrational frequency of ions and is different from ion hopping among different sites. The Li^+ probability density, which is calculated as the fraction of time the Li ion occupied each spatial position (Figure 2b,c), has an ellipsoid-like (as in LGPS and LLZO) or an irregularly elongated Li^+ probability

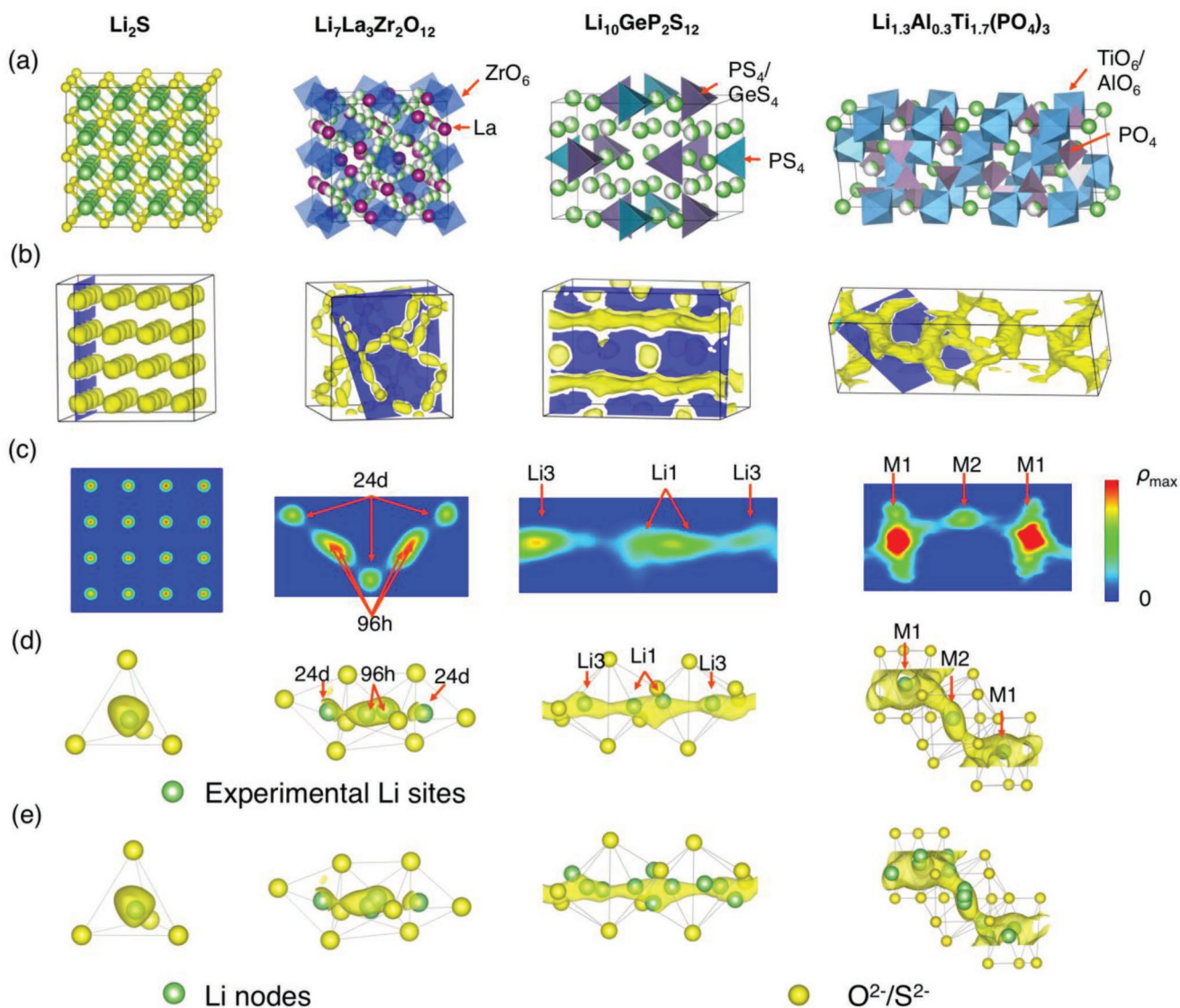


Figure 2. Li-ion probability density and Li sites of non-SIC versus SICs. a) Crystal structures of Li_2S , $\text{Li}_7\text{La}_3\text{Zr}_2\text{O}_{12}$ (LLZO), $\text{Li}_{10}\text{Ge}(\text{PS}_6)_2$ (LGPS), and $\text{Li}_{1.3}\text{Al}_{0.3}\text{Ti}_{1.7}(\text{PO}_4)_3$ (LATP). b) Li^+ probability density from AIMD simulations at 900 K. c) The cross-section of Li^+ probability density from the blue plane in (b). ρ_{\max} refers to the highest Li^+ probability in the cross-section. Comparison of Li^+ probability density between d) Li sites from diffraction experiments and e) Li nodes predicted from topological analysis. In SICs, the Li^+ probability density shows significant positional disordering of Li ions around the enlarged sites with a large local space. All isosurface is the average probability density in the material.

density (as in LAMP), suggesting positional disordering of the Li ion. The nonspherical shape of these Li⁺ probability densities from AIMD simulations also agrees with ion nuclear density obtained from neutron diffraction analyses in previous studies.^[7,29,33–38]

As a result of this positional disordering, this enlarged site is commonly treated and fitted as split sites in Rietveld refinement of diffraction experiments. The experimentally determined structures of most SICs have split Li sites (Figure 2d),^[24,37–40] For example, LGPS has two neighboring split Li1 sites within a short distance of 1.5 Å and a partial occupancy of 0.466,^[38] which correspond to a Li-ion probability density with an elongated ellipsoid shape (Figure 2) and agree with the ion nuclear density from neutron diffraction experiments.^[36,37] Similarly, cubic phase LLZO has two neighboring 96h sites only 0.8 Å apart with a partial occupancy of 0.44.^[40] The physical meaning of these closely spaced split sites with partial occupancy is the positional disordering of Li ion as shown by the Li⁺ probability density from AIMD simulations (Figure 2) and by the ion nuclear density from neutron diffraction.^[29,35,41,42] This positional disordering on enlarged Li sites is also reflected as a large or anisotropic atomic displacement parameter (ADP) in fitting the diffraction patterns of these structures.^[29,35,37,42] Site splitting or ADP, which are commonly used for better fitting such enlarged Li sites in SICs, are usually not necessary for typical materials.^[35] For example, in Li₂S, the thermal vibration of Li ions is centered to the equilibrium sites, corresponding to spherical, symmetric, localized Li⁺ probability density (Figure 2c). Therefore, the enlarged Li site is a unique feature in SICs.

This positional disordering of enlarged Li site is directly related to the large local space in the crystal structural frameworks of the SICs. In the crystal structural frameworks of the SICs, the polyanion groups are arranged in a specific manner (More details provided in the Supporting Information) so as to provide a large local space for accommodating a Li ion in a range of positions. The enlarged site is confirmed by the presence of a group of Li nodes (definition and description is provided in the Experimental Section) in the crystal structural framework, which indicates a large local space (Figure 2e). As shown in the next subsections, LGPS, LLZO, and LAMP have enlarged Li sites with sizes of 3.3, 2.4, and 5.2 Å, respectively. Therefore, the enlarged Li site is a direct result of these unique crystal structural frameworks (Section 2.2). The unique enlarged Li sites in SICs may represent a locally flat energy landscape and enhance the disordering of Li sublattice for fast ion conduction in SICs, as further elaborated in Section 3. In summary, the enlarged Li sites in SICs are consistently reflected as large local spaces in the crystal structural framework, an elongated Li probability density as observed in real-time Li⁺ dynamics from AIMD simulations, and the partially occupied neighboring sites and ion nuclear density from diffraction experiments.

2.2. Topological Analysis of Crystal Structural Framework

Using topological analysis (Experimental Section), we analyzed the local space in crystal structural framework that can be occupied by Li ions. As shown in LGPS (Figure 3), LLZO (Figure 2e),

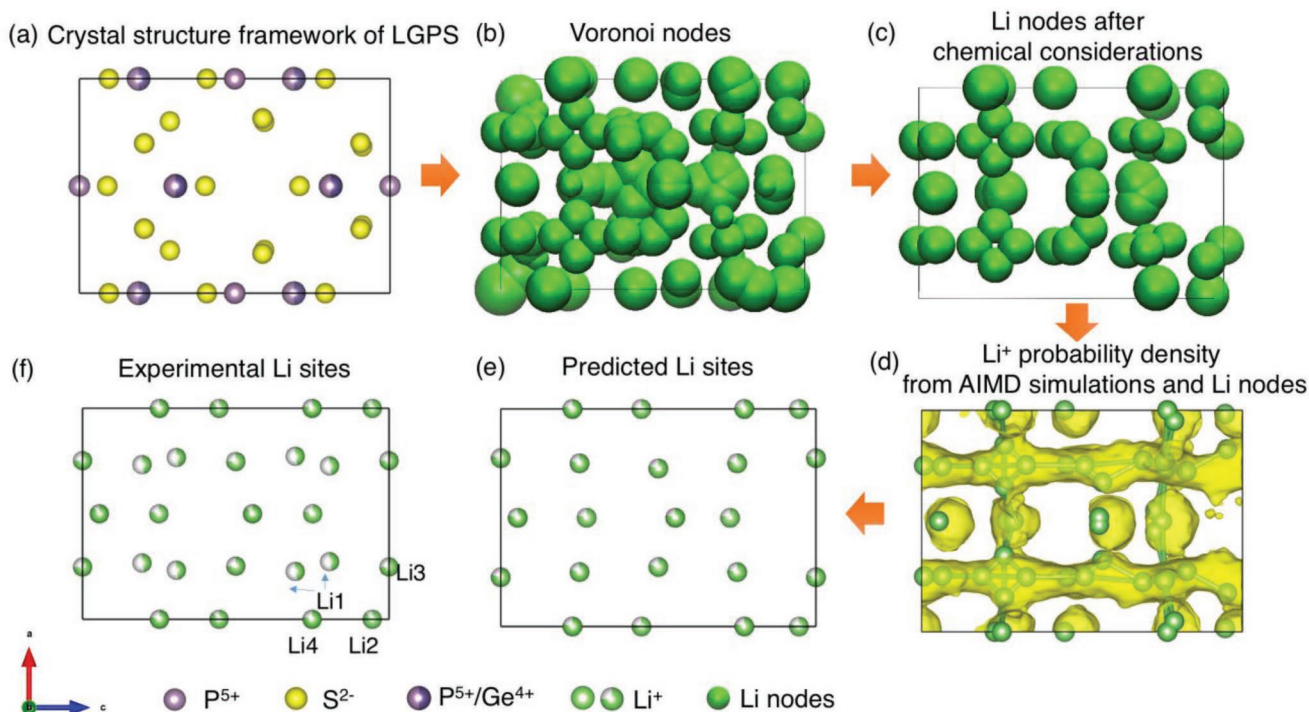


Figure 3. Topological analysis of LGPS. a) Crystal structure framework of LGPS after removing all Li ions. b) Voronoi nodes (green) with radii representing local space in the crystal structural framework. c) Li nodes after considering the chemical environment such as bond valence and cation distances. d) Li⁺ probability density (yellow) from AIMD simulation at 900 K and Li nodes (green spheres) and their connections (bars) representing the Li⁺ diffusion channels. e) Predicted Li sites from groups of Li nodes in agreement with f) experimental Li sites.

and LATP (Figure 2e), the topological analyses of the non-Li crystal structural framework provide Li nodes and diffusion channels (Figure 3d), which are in good agreement with experimental sites from diffraction characterization (Figure 3e,f) and Li⁺ probability density from AIMD simulations (Figure 3d). For example, in LGPS, the predicted Li sites (Figure 3e) agree well with experimental Li1 to Li4 sites in LGPS (Figure 3f).^[36–38] It is worth mentioning that the Li4 site was previously neglected in the earliest reports of the LGPS structure,^[36–38] but our topological analyses were able to successfully predict this site based on the non-Li crystal structural framework. In addition, the network of Li⁺ diffusion channels, as formed by connecting the Li nodes, agrees well with the actual diffusion channels shown by Li⁺ probability density from AIMD simulations (Figure 3d). Therefore, topological analysis of the crystal structural framework with basic chemical considerations reproduces Li sites and Li⁺ diffusion channels. These agreements demonstrate the intrinsic physical correlation of the Li sublattice and diffusion network with the crystal structure framework.

The topological analysis revealed that the enlarged Li site in LGPS, which is represented as two neighboring Li1 sites from experiments (Figure 3f), is a large local space for occupying a Li ion, as shown by a group of four Li nodes with large radius (Figure 3d). Due to the Li⁺ positional disordering on this local space (Figures 2 and 3), the group of Li nodes is treated as a single enlarged Li site (Figure 3e) calculated with a size of 3.3 Å (Topological Analysis of Crystal Structural Framework section in the Experimental Section). Therefore, the enlarged Li site originates from the large local space within the crystal structural framework. Similarly, the topological analysis also confirmed that the enlarged sites in other SICs such as 96h sites in LLZO and M1 sites in LATP also correspond to a large local space (Figure 2). A quantitative analysis of these enlarged Li sites in a large number of materials is shown in Section 2.3.

2.3. Quantifying Crystal Structural Framework

To quantify the key features of crystal structural frameworks of fast ion conductors, we performed topological analyses on all Li-containing oxides and sulfides from the ICSD.^[43] We first quantified the percolation radius of diffusion channels, which is crucial for the Li⁺ migration barrier. The percolation radius is defined as the maximum radius of a sphere that can percolate across at least one direction of the structure. The percolation radii for oxides and sulfides are summarized in Figure 4a,b. The percolation radii are 0.54, 0.62, and 0.72 Å for garnet LLZO, LISICON Li_{1.4}Zn(GeO₄)₄,^[44] and NASICON Li_{1.2}Al_{0.2}Ge_{0.2}Ti_{1.6}(PO₄)₃,^[45] respectively. The percolation radii are 0.61, 0.64, 0.67, and 0.58 Å for LGPS, Li₇P₃S₁₁,^[46] β-Li₃PS₄,^[47] and LiZnPS₄,^[48] respectively. We found that the percolation radii of known SICs fall within a narrow range of 0.54–0.72 Å (Figure 4a,b). This observation confirms that the diffusion channel size of SICs should not be too small or too large for low-barrier ion migration.^[22,23]

A 3D-connected diffusion network in the crystal structural framework is crucial for fast ion conductors. As shown in our topological analysis (Section 2.2), the connection of Li nodes, which are spaces to accommodate Li ions, can accurately represent Li⁺ diffusion channels, consistent with Li⁺ probability

density from AIMD simulations (Figures 2 and 3). For those materials with decent percolation radii within the aforementioned range, we quantify the connectivity of Li nodes in crystal structural framework by calculating the minimum distance *d* that can connect Li nodes to form a 3D percolation network (Section 2.2). The node–node connection provides a good representation of diffusion pathways, as Li nodes directly correspond to the local space for Li ions (Figure 3d). A short distance *d* suggests good connectivity of the Li diffusion network and a likely low energy barrier for ion hopping. Among these materials, we found only small distances of 2.2, 1.9, and 1.9 Å are needed to connect Li nodes in LGPS, LLZO, and LATP, respectively. In all SIC compounds, Li nodes form a 3D percolation network with a minimum node distance of less than 2.5 Å (Figure 4c,d).

The enlarged Li site with large size was identified in Section 2.1 as a key feature of SICs. For materials with both good percolation radius and good diffusion network, we analyzed the size of the large Li site and found that the size of the enlarged site in known SICs is larger than other materials. For example, the size of the largest site is 3.3, 2.4, and 5.2 Å for LGPS, LLZO, and NASICON LATP, respectively (Figure 4e,f). Therefore, the enlarged Li site is given by a large local space of crystal structural framework and is a key feature of SIC materials.

In summary, a few key features of the crystal structural frameworks of SICs were quantified and identified in our topological analyses. Most SICs have a percolation radius of 0.5–0.75 Å and enlarged Li sites with a local space size larger than 2.2 Å to host Li ions. In addition, the Li nodes in SICs are connected by a short distance of <2.5 Å, forming a well-connected diffusion network. From our histograms, we find that a large number of materials can satisfy these features, suggesting an opportunity for materials discovery.

2.4. High Throughput Screening for Fast Li-Ion Conductors

Here, using the identified features of structures, we performed high-throughput screening for the crystal structure frameworks that shared the same features of known Li-ion conductors. Our high-throughput screening started with all Li-containing oxides and sulfides, a total of 5537 and 510 compounds, respectively, from the ICSD. The screening steps are described as follows. The cutoff values of each screening criteria were chosen based on the value ranges of known SICs identified in Section 2.3. The compounds that passed each screening step are summarized in Figure 5 and Tables S1–S6, Supporting Information.

Step 1. Basic Materials Check: We excluded the compounds that have any of the following attributes: having number of elements <3, containing radioactive elements, having no or wrong oxidation states, containing water molecules (i.e., hydrates), containing anion sites with disordering or partial occupancy, containing more than one anion species, and having more than 500 sites. This step leads to 2866 oxides and 157 sulfides to further screen by topological analyses.

Step 2. Percolation Radius: To have low migration energy, the structures require an adequately large percolation radius. We selected the compounds with a percolation radius of >0.5 Å for oxides and >0.55 Å for sulfides.

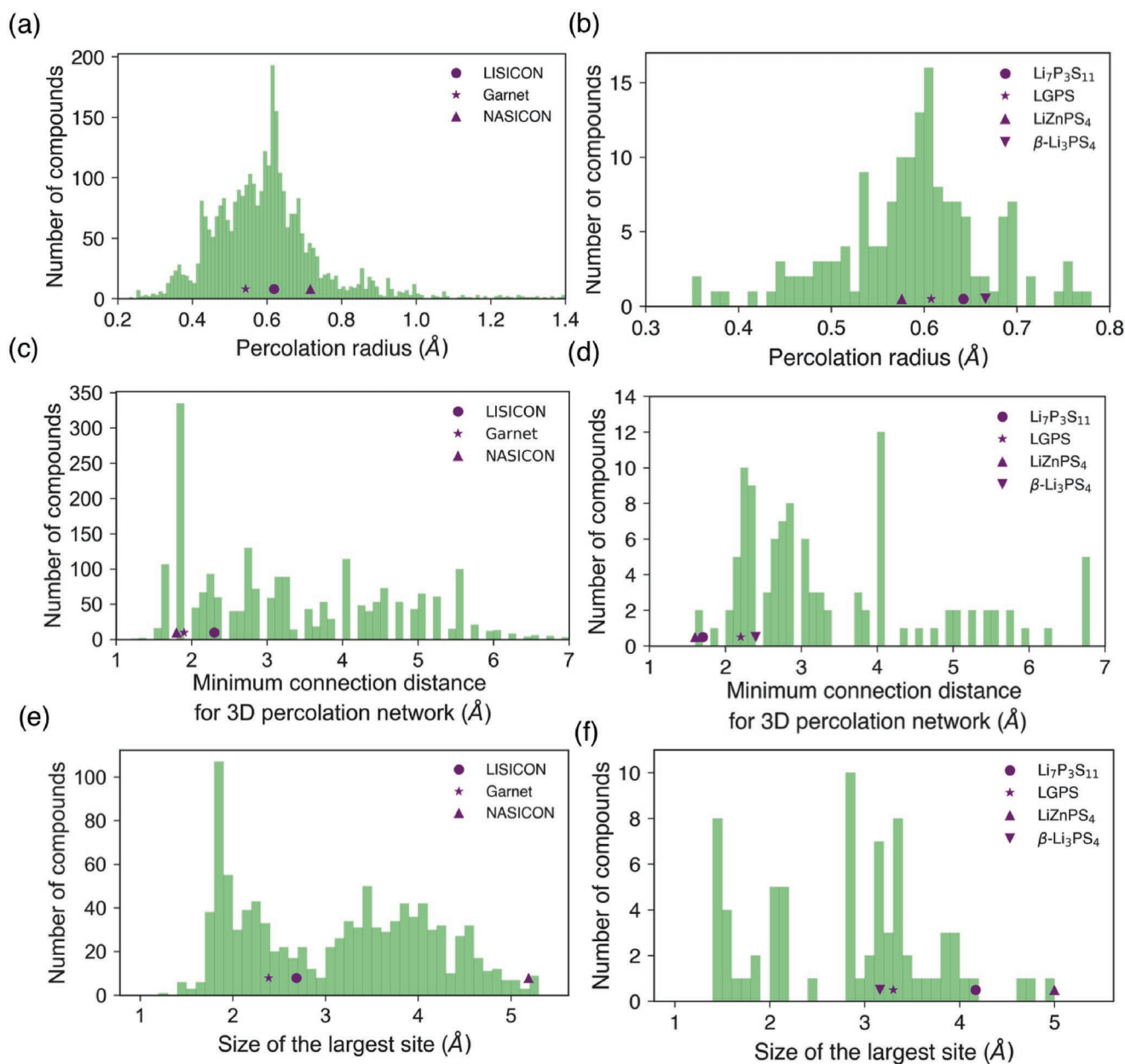


Figure 4. Histograms of the features of crystal structural framework of Li-containing oxides and sulfides. The percolation radius of the crystal structural framework for a) oxides and b) sulfides. Minimum connection distance of Li nodes for forming a 3D percolation network in c) oxides and d) sulfides with good percolation radius. Size of the site with largest size in e) oxides and f) sulfides with good percolation radius and 3D connection network. Values for representative SICs, e.g., LGPS, LISICON ($\text{Li}_{14}\text{Zn}(\text{GeO}_4)_4$), garnet ($\text{Li}_7\text{La}_3\text{Zr}_2\text{O}_{12}$), and NASICON ($\text{Li}_{1.2}\text{Al}_{0.2}\text{Ge}_{0.2}\text{Ti}_{1.6}(\text{PO}_4)_3$), are marked.

Step 3. 3D Diffusion Network: The structures should have a 3D-connected diffusion network and we screened for those structures in which Li nodes are connected with a minimum distance of $<3 \text{ \AA}$.

Step 4. Enlarged Li Site: Since the enlarged Li site is a feature of SICs, we selected crystal structural frameworks that have enlarged Li sites with a size of $>2.2 \text{ \AA}$ (Topological Analysis of Crystal Structural Framework section in the Experimental Section). 704 oxides and 40 sulfides (Tables S3 and S4, Supporting Information) passed these three criteria (Steps 2–4) out of 2866 oxides and 157 sulfides (after Step 1) analyzed.

Step 5. Practical Considerations: We excluded a few well-explored ternary oxide systems and some oxides with certain elements. We excluded the following compounds: all Li–X–O ternary compounds, where X is S, I, Si, C, P, Al, Ge, Se, B, or Cl, and Li–P–S; oxide compounds containing certain transition metal elements, such as Fe, Mn, Ni, Ti, Mo, V, or Co, or containing N, Re, Ho, Hf, Ru, Eu, Lu; compounds in which Li and other elements share the same site, which may block Li diffusion channel. These excluded compounds are in Tables S5 and S6 in the Supporting Information.

Inorganic Crystal Structure Database (ICSD)

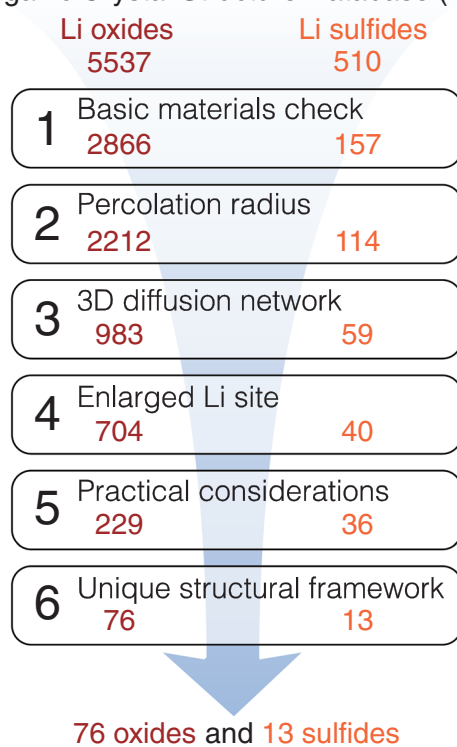


Figure 5. Workflow of high-throughput screening of Li-containing oxides and sulfides for crystal structure frameworks with the same features of known Li-ion conductors.

Step 6. Unique Structure Framework: We grouped the compounds that have the same crystal structural framework regardless of ionic species and represented each group with a unique crystal structure framework.

In summary, our high-throughput screening obtained 76 and 13 unique crystal structural frameworks of oxides and sulfides that shared the same features as known fast Li-ion conductors, as summarized in **Table 1** with representative compounds for each unique crystal structural framework. The list of all compounds that adopt each unique crystal structural framework is provided in Tables S2–S4 in the Supporting Information. Among them, there are known SIC oxides, such as lithium garnet, NASICON, $\text{Li}_3\text{M}_2(\text{PO}_4)_3$ ($\text{M} = \text{Fe}, \text{Sc}, \text{Cr}$),^[49,50] and LISICON, and known SIC sulfides, such as LGPS, LiZnPS_4 , $\text{Li}_7\text{P}_3\text{S}_{11}$, and $\beta\text{-Li}_3\text{PS}_4$ (Table S2, Supporting Information). In addition to those SICs summarized in Table 1, other known fast ion conductors such as perovskite $\text{Li}_x\text{La}_{2/3-x/3}\text{TiO}_3$ (LLTO), β -alumina,^[51] argyrodite $\text{Li}_6\text{PS}_5\text{X}$ ($\text{X} = \text{Cl}, \text{Br}, \text{I}$),^[52] and antiperovskite Li_3OCl ^[53] also meet most structural screening criteria. LLTO and lithium β -alumina were excluded as 2D conductors, although exhibited other key features such as large percolation radius and enlarged Li site. Argyrodite $\text{Li}_6\text{PS}_5\text{X}$ ($\text{X} = \text{Cl}, \text{Br}, \text{I}$) and antiperovskite Li_3OCl (Figure S7, Supporting Information) were excluded as mixed-anion systems but would otherwise pass all screening criteria. In summary, our high-throughput screening uncovered crystal structural frameworks of known SICs and discovered

potential new fast Li-ion conductors that exhibit similar percolation radii, good diffusion networks, and enlarged Li sites.

2.5. New Li-Ion Conductors

We further performed AIMD simulations to evaluate Li-ion diffusion in the structures obtained from high-throughput screening. For each crystal structural framework, we selected one representative composition (Tables S7 and S8, Supporting Information). Since an appropriate level of Li content is required to activate fast ion diffusion in crystal structural framework, we applied aliovalent substitution to change the Li concentration (see Experimental Section) until the averaged Li occupancy, which is the ratio between the number of Li ions and the total number of predicted Li sites, reached the range of 0.5–0.8. For most compounds studied, Li content is increased to fill newly predicted Li sites in the crystal structural framework. This substitution strategy is based on the previously demonstrated successes of cation substitution in crystal structural framework to achieve SICs, such as Li stuffing in the garnet structure $\text{Li}_3\text{M}_3\text{Te}_2\text{O}_{12}$ ($\text{M} = \text{La}, \text{Y}, \text{Pr}, \text{Nd}$) to LLZO^[20] and in NASICON structure $\text{LiTi}_2(\text{PO}_4)_3$ to LATP.^[19] As shown by He et al.,^[24] inserting Li ions into high-energy sites may activate a concerted migration of multiple Li ions and significantly decrease the migration energy barrier. The calculated energy above hull E_{hull} of doped compositions are summarized in Tables S7 and S8 in the Supporting Information. Only those doped compounds with a reasonable phase stability of $E_{\text{hull}} < 50$ meV per atom were further studied for ion diffusion in AIMD simulations.

In order to screen a large number of candidates with limited computational resources, we adopted a scheme of AIMD simulations to calculate the Li^+ conductivity at two temperatures 1150 and 900 K (First Principles Computation Screening of New Materials section in the Experimental Section). The results are plotted according to the conductivity at two temperatures similar to ref. [54]. Those compounds falling within the light blue region (**Figure 6**) may have extrapolated Li^+ conductivity of >0.1 mS cm^{-1} at 300 K and all known SICs fall within this region. The ability to uncover known SICs validates our screening scheme consisting of high-throughput structural analyses, DFT calculations of materials substitution, and AIMD simulations.

Our AIMD simulation screening identified 15 candidates that are predicted to have extrapolated Li^+ conductivity of >0.1 mS cm^{-1} at 300 K. The exact compositions, substitution methods, phase stabilities, and calculated diffusional properties of these fast Li-ion conductors are summarized in **Table 2** with the Arrhenius plots shown in Figure S8 in the Supporting Information. Among these compounds, the doped LiTaSiO_5 and doped Li_6KBiO_6 show highest predicted Li^+ conductivity of >1 mS cm^{-1} at 300 K, comparable to known oxide SICs. These doped compounds all have decent phase stability with $E_{\text{hull}} < 50$ meV per atom. Better substitution strategies may be further explored to optimize stability and Li-ion conductivity. Some compounds have expensive or toxic elements such as In, or Pb, and other compositions in the same structures can be explored to replace the undesirable elements.^[21,55]

Table 1. High-throughput screening results for the crystal structural frameworks of potential Li-ion conductors. Each unique crystal structural framework may have a number of compositions (Tables S2–S4, Supporting Information). Compounds that pass further AIMD screening for high Li⁺ conductivity are highlighted.

	ICSD ID	Composition	ICSD ID	Composition	ICSD ID	Composition
Known SICs	100169	Li _{3.5} Zn _{0.25} GeO ₄	69763	LiGe ₂ (PO ₄) ₃	422259	Li ₇ La ₃ Zr ₂ O ₁₂
	50420	Li ₃ Sc ₂ (PO ₄) ₃	180319	Li ₃ PS ₄	95785	LiZnPS ₄
	188887	Li ₁₀ GeP ₂ S ₁₂	157654	Li ₇ P ₃ S ₁₁		
Compounds with high potential to be SICs	635	Li ₂ Hg(PO ₃) ₄	51754	Li ₃ Al(BO ₃) ₂	192496	Li₂B₃PO₈
	1044	Li ₂ WO ₄	59640	Li ₄ Zn(PO ₄) ₂	195819	Li ₂ Ga ₂ GeS ₆
	1045	Li ₂ WO ₄	60948	Li₃In₂(PO₄)₃	200520	LiPr(WO ₄) ₂
	1123	LiP ₃ PbO ₉	65260	Li ₄ KAlO ₄	202116	Li ₃ NaGeO ₄
	1411	Li ₄ PbO ₄	65764	LiZnPO ₄	237524	Li₃CuB₃O₇
	1485	Li ₂ TeO ₄	66137	LiAlSiO ₄	238234	Li ₂ FeGeS ₄
	1897	Li ₂ W ₂ O ₇	67535	LiGeBO ₄	241234	Li₃Sc(BO₃)₂
	2149	LiCuP ₃ O ₉	67991	Li ₁₄ Be ₅ B ₁₀ O ₂₇	247216	Li ₆ CuB ₂ O ₁₀
	2929	LiAlSiO₄	68653	Li ₆ Y(BO ₃) ₃	248343	Li ₃ B(PO ₄) ₂
	4317	Li ₂ TeO ₃	71035	Li₆KBiO₆	249215	Li ₆ CuB ₄ O ₁₀
	8237	Li₂ZnSiO₄	72098	Li ₃ AlGeO ₅	250678	Li ₂ TeWO ₆
	14235	LiAlSi ₂ O ₆	73124	Li ₄ KNbO ₅	262642	Li₂In₂Si₆
	15395	Li ₂ WO ₄	73150	Li ₅ B ₇ S ₁₃	279578	Li ₂ Al(BO ₃) ₅
	15415	LiAl(Si ₂ O ₅) ₂	73151	Li ₉ B ₁₉ S ₃₃	291512	Li₂NaB(PO₄)₂
	26451	Li ₂ Te ₂ O ₅	74860	LiAl(PO ₃) ₄	291513	LiNa₂B₅(PO₇)₂
	26836	Li ₄ SiGe ₃ O ₁₀	78326	Li₁₀Si₂PbO₁₀	380104	Li ₃ BS ₃
	30909	Li ₃ Ba ₂ (PO ₃) ₇	79098	Li ₁₂ CsNa ₃ (GeO ₄) ₄	413371	Li₇NbO₆
	31316	LiScO ₂	79352	LiZnPO ₄	415208	LiEuPS ₄
	31941	Li ₂ ZrO ₃	79616	LiSr(BS ₂) ₃	415336	Li ₉ Nd ₂ (PS ₄) ₅
	35250	Li ₁₄ K ₂ Pb ₃ O ₁₄	82277	LiBiO ₃	416877	LiLa(PO ₃) ₄
	35252	Li ₈ Nb ₂ O ₉	86458	Li ₃ Sc ₂ (PO ₄) ₃	417653	Li ₆ Y ₃ (PS ₄) ₅
	36475	Li_{2.1}W_{0.9}Nb_{0.1}O₄	88785	Li ₂ GeTeO ₆	423127	LiIn(WO ₄) ₂
	37084	Li ₃ KPbO ₄	90849	LiSi ₂ BO ₆	424079	Li ₂ B ₈ SeO ₁₅
	38250	LiK(PO ₃) ₂	91496	LiScP₂O₇	424834	Li ₃ SbS ₃
	38324	Li ₃ KGeO ₄	92708	LiAlSiO ₄	425763	Li₄MnGe₂S₇
	39464	LiNbGeO₅	93013	LiBa(B ₃ O ₃) ₃	427399	LiCs(B ₃ O ₃) ₂
	39648	LiTaSiO₅	94355	Li ₃ In(BO ₃) ₂	429249	Li ₃ AsW ₇ O ₂₅
	40245	Li ₃ BiO ₃	96914	LiGaS ₂		
	50612	Li ₂ AlBO ₄	97909	LiAlSiO ₄		
	50950	LiZnPO ₄	172184	Li₉Ga₃P₈O₂₉		
51314	LiAlB ₂ O ₅	182033	LiNbO ₃			

The materials that do not show high extrapolated ionic conductivity of >0.1 mS cm⁻¹ at 300 K are shown in the white region of Figure 6 and are listed in Tables S9 and S10 in the Supporting Information. Given our limited computation tests, we only explored a few substitution elements and compositions. For some crystal structural frameworks that exhibited poor diffusion, good ion conductors may be possible in different compositions using different substitution methods. For those doped compositions that are excluded due to poor phase stability, different substitution methods may achieve compositions with good stability. Further studies are needed to identify and optimize the compounds to design fast ion conductors.

3. Discussion and Conclusion

In this study, we systematically quantified the crystal structural frameworks of lithium SICs, and identified their unique features that result in fast Li-ion conduction. One of the newly noted key features is the enlarged Li site given by large local space of crystal structures promoting Li disordering. As revealed by the topological analysis, the enlarged Li site corresponds to a large local space larger than 2.4 Å in size and can be occupied by Li ion at multiple positions within a very close distance. Li ions move rapidly within the enlarged site, in contrast to thermal vibration centered to the equilibrium

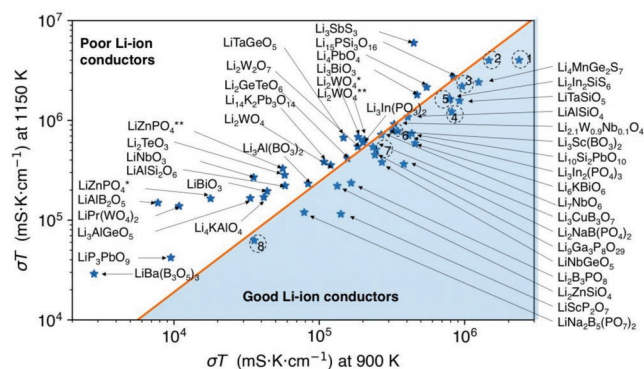


Figure 6. Screening results of AIMD simulations. The product of conductivity and temperature at 900 and 1150 K for known Li SICs and the representative compounds of newly predicted structures (legend in original composition). The light blue region corresponds to the region of extrapolated $\sigma_{300K} > 0.1 \text{ mS cm}^{-1}$ from the conductivities at 1150 and 900 K. Polymorphic structures are asterisked: LiZnPO_4^* (ICSD-50950), LiZnPO_4^{**} (ICSD-79352), Li_2WO_4^* (ICSD-1044), and $\text{Li}_2\text{WO}_4^{**}$ (ICSD-1045). The known SICs are numbered: 1) $\text{Li}_7\text{P}_3\text{S}_{11}$, 2) $\beta\text{-Li}_3\text{PS}_4$, 3) $\text{Li}_2\text{Zn}_{0.5}\text{PS}_4$, 4) LGPS, 5) LISICON: $\text{Li}_{1.4}\text{Zn}(\text{GeO}_4)_4$, 6) $\text{Li}_{1.3}\text{Al}_{0.3}\text{Ti}_{1.7}(\text{PO}_4)_3$ (LATP), 7) $\text{Li}_7\text{La}_3\text{Zr}_2\text{O}_{12}$ (LLZO), and 8) $\text{Li}_{5/16}\text{La}_{9/16}\text{TiO}_3$ (LLTO).

positions of a regular site. As observed in AIMD simulations, Li ions occupy a spread of spatial positions within the enlarged site over a short period of time, forming an elongated, nonsymmetrical Li-ion probability density (Figure 2) or ion nuclear density. In the crystal structures determined by Rietveld refinement from diffraction experiments, such enlarged Li sites show high anisotropy and large ADP, and are often fitted as multiple partially occupied close-neighboring sites, as reported in LGPS, garnet LLZO, and argyrodite.^[29,35–38,40–42,56,57] Further studies are still needed to understand the mechanisms of the enlarged Li site and Li positions in specific crystal structures and to experimentally verify them using local characterization techniques.

Table 2. New Li-ion conductors predicted by AIMD simulations.

ICSD ID	Original composition	Doped composition	E_{hull} [meV per atom)	E_a [eV]	σ at 300 K [mS cm ⁻¹]	Error bound [σ_{min} , σ_{max}] [mS cm ⁻¹]
2929	LiAlSiO_4	$\text{Li}_{1.25}\text{Al}_{1.25}\text{Si}_{0.75}\text{O}_4$	42	0.28 ± 0.02	1.3	[0.65, 2.8]
8237	$\text{Li}_2\text{ZnSiO}_4$	$\text{Li}_{2.5}\text{Zn}_{0.75}\text{SiO}_4$	12	0.20 ± 0.06	3.1	[0.28, 35]
39464	LiNbGeO_5	$\text{Li}_{1.25}\text{Nb}_{0.75}\text{Sn}_{0.25}\text{GeO}_5$	31	0.30 ± 0.04	0.24	[0.046, 1.2]
39648	LiTaSiO_5	$\text{Li}_{1.5}\text{Ta}_{0.5}\text{Zr}_{0.5}\text{SiO}_5$	28	0.23 ± 0.02	6.4	[3.0, 14]
60948	$\text{Li}_3\text{In}_2(\text{PO}_4)_3$	$\text{Li}_{3.5}\text{In}_2\text{P}_{2.5}\text{Ge}_{0.5}\text{O}_{12}$	29	0.26 ± 0.03	1.4	[0.46, 4.4]
71035	Li_6KBiO_6	$\text{Li}_{6.5}\text{KSn}_{0.5}\text{Bi}_{0.5}\text{O}_6$	22	0.21 ± 0.02	5.7	[2.1, 16]
78326	$\text{Li}_{10}\text{Si}_2\text{PbO}_{10}$	$\text{Li}_9\text{SiPPbO}_{10}$	8	0.35 ± 0.04	0.14	[0.027, 0.67]
91496	LiScP_2O_7	$\text{Li}_{1.33}\text{ScSi}_{0.33}\text{P}_{1.67}\text{O}_7$	32	0.28 ± 0.07	0.17	[0.009, 3.3]
172184	$\text{Li}_9\text{Ga}_3\text{P}_8\text{O}_{29}$	$\text{Li}_{9.5}\text{Ga}_3\text{Ge}_{0.5}\text{P}_{7.5}\text{O}_{29}$	40	0.33 ± 0.06	0.12	[0.01, 1.4]
237524	$\text{Li}_3\text{CuB}_3\text{O}_7$	$\text{Li}_{3.17}\text{CuB}_{2.83}\text{Be}_{0.17}\text{O}_7$	50	0.31 ± 0.06	0.32	[0.027, 3.7]
241234	$\text{Li}_3\text{Sc}(\text{BO}_3)_2$	$\text{Li}_{3.375}\text{Mg}_{0.375}\text{Sc}_{0.625}(\text{BO}_3)_2$	21	0.37 ± 0.06	0.10	[0.0062, 0.80]
262642	$\text{Li}_3\text{In}_2\text{SiS}_6$	$\text{Li}_3\text{Al}_3\text{S}_6$	0	0.32 ± 0.03	0.53	[0.13, 2.2]
291512	$\text{Li}_2\text{NaB}(\text{PO}_4)_2$	$\text{Li}_{2.25}\text{NaB}(\text{P}_{0.875}\text{Ge}_{0.125}\text{O}_4)_2$	41	0.26 ± 0.06	1.0	[0.083, 12]
291513	$\text{LiNa}_2\text{B}_5(\text{PO}_7)_2$	$\text{Li}_2\text{Na}_2\text{BeB}_4(\text{PO}_7)_2$	41	0.30 ± 0.06	0.14	[0.011, 1.7]
425763	$\text{Li}_4\text{MnGe}_2\text{S}_7$	$\text{Li}_6\text{MgAl}_2\text{S}_7$	0	0.31 ± 0.05	1.2	[0.18, 7.7]

Having Li ions at multiple positions promotes the disordering of Li sublattice, since the multiple positions of Li ions and their fast movements among them significantly increase the entropy of Li sublattice.^[28] In addition, the significantly increased flexibility of Li-ion positions in large sites leads to an energy degeneracy of the Li sublattice, i.e., a large number of configurations exhibits similar energies, which induces geometrical frustration of the Li sublattice.^[27–29,58,59] The strong Coulombic interactions among Li ions further complicate the energetics of the Li sublattice. For example, in garnet LLZO (Figure 1), the Li-ion configuration has a known pattern where an occupied $24d$ site leads to unoccupied nearest-neighbor $96h$ sites, but occupied next nearest-neighbor $96h$ sites, as a rearrangement within an enlarged site (i.e., two $96h$).^[35] The resulting configuration of the Li sublattice may exhibit an incompatible symmetry with the crystal structural framework, thus inducing geometrical frustration of the Li sublattice as revealed in lithium garnet.^[27,29] Therefore, the enlarged Li site promotes the disordering of the Li sublattice in SICs.

The enlarged Li sites and disordered Li sublattice also facilitate Li-ion diffusion. Li ions migrate easily within the enlarged site, and these enlarged sites have good connectivity with other sites to percolate through the structure. Furthermore, in a disordered Li sublattice, a large number of different Li configurations provide a variety of Li-ion hopping modes between many possible disordered Li-ion configurations (Figure 1). The ion diffusion pathway with the lowest energy barrier would occur with an exponentially higher rate according to the Arrhenius relation. As a general phenomenon, frustrated systems for a wide range of physical phenomena are featured with correlated transition between states.^[27–29,58,59] As reported in previous studies, the dominant diffusion mechanism in SICs is the concerted migration of multiple Li ions,^[24–26,28] which can be understood as a correlated transition between two Li^+ configurations. Such correlated transition has a low migration barrier in a disordered sublattice (Figure 1).^[24] In contrast, for an ordered Li sublattice with one symmetric ground-state

configuration, the ion migration mode is limited to the isolated, individual ion hopping, which often has a higher energy barrier (Figure 1). The disordering of the Li sublattice plays an important role in activating multi-ion concerted migrations with low barrier and in enabling a super-ionic conductor.

In this study, topological analyses of crystal structural framework with basic chemical considerations are demonstrated as a highly effective technique to quantitatively describe and identify local space for Li occupancy, Li site, and Li diffusion channels, which have good agreements with *ab initio* calculations and diffraction experiments. Such simple topological analysis can serve as a useful tool for predicting Li sites in complex structures and for quantitatively understanding the local space in crystal structures. This technique can be further extended to a wide range of ionic materials with mobile Na, Mg, O, F, and H ions.

Our high-throughput topological analyses on all known Li-containing oxides and sulfides, including SICs, provide quantitative understanding of crystal structures. All SIC oxides and sulfides have crystal structural frameworks with decent percolation radius of 0.5–0.75 Å, well connected diffusion networks with a Li-node distance of <2.5 Å, and an enlarged Li site of >2.2 Å in size. According to topological analysis, the enlarged site is a result of a slightly distorted anion polyhedron that provides a large space for accommodating Li ions at multiple positions. This may explain why the crystal structures of known SICs, such as LGPS, LLZO, and NASICON, have such large unit cells and are distorted compared to close-packed structures, whereas highly symmetrical crystal structures are generally more closely packed and do not have large local space for such enlarged Li sites.

Our high-throughput screening has identified all crystal structures that exhibit features similar to those of known SICs and has confirmed that many of these structures are good Li-ion conductors with increased Li concentration after aliovalent substitution. In our identified structures, we found that a large number of these crystal structures are based on polyanion groups of P, Si, Ge, or B, which can form complex crystal structure frameworks with the required combination of percolation radius, enlarged site, and diffusion network connectivity. Some of these compounds may be difficult to synthesize especially at high substitution concentration, due to the favorable formation of stable impurity phases, such as phosphate, silicate, and borate. Our high-throughput screening also found some compounds with less explored cations, such as Sc, Y, In, Nb, and W, may provide desirable crystal structural frameworks. Some excluded structures with transition metal elements (summarized in Tables S5 and S6, Supporting Information) may also have good frameworks for fast ion conduction. For example, the well-known Li-ion conducting Chevrel phase, LiMo_6S_8 , was found to contain all required features of SICs. In summary, our high-throughput computational screening uncovered many new structures that have the potential to be fast Li-ion conductors. For each crystal structural framework, there are a number of compounds and many possible doped compositions. For example, lithium garnet and NASICON are known to have a wide range of cation and Li concentrations combinations in their crystal structure frameworks. In addition, given the elements in some compounds may be expensive, toxic, or difficult to synthesis, the exploration of different cations as substitutions

may be essential for practical usage of the materials. Since we only screened a small number of doped compositions, many potential compositions that may have better stability or conductivity have yet to be identified. Our work only studied known existing crystalline structures, and there is great promise in the exploration and discovery of new crystal structures, amorphous glass materials, and novel mesoscale materials. Furthermore, for the ion conductors to be used as solid electrolytes, many additional properties such as electrochemical stability and interface compatibility need to be considered (Supporting Information). Nevertheless, our study provides valuable resources for further computation and experiments to design and discover new Li-ion conductors.

4. Experimental Section

First Principles Computation: All DFT calculations in this study were performed using Vienna *ab initio* simulation package^[60] within the projector augmented-wave approach. Perdew–Burke–Ernzerhof^[61] functionals based on generalized-gradient approximation were adopted. The parameters in static DFT calculations were consistent with the *Materials Project*.^[39,62,63]

Ab Initio Molecular Dynamics Simulation: AIMD simulations were performed in supercell models using nonspin-polarized DFT calculations with a Γ -centered *k*-point. The time step was set to 2 fs. The initial structures were statically relaxed and were set to an initial temperature of 100 K. The structures were then heated to targeted temperatures at a constant rate by velocity scaling during 2 ps. During the estimation of Li-ion diffusion, NVT ensemble (fixed number of atoms, volume and temperature) using Nosé–Hoover thermostat^[64] was adopted. The total time of AIMD simulations were in the range of 100–1000 ps until the diffusivity was converged. The ionic diffusivity and conductivity were calculated following the established method in ref. ^[65]. The probability density of Li ion was calculated as the fraction of time that each spatial location is occupied.^[24]

First Principles Computation Screening of New Materials: For each crystal structural framework identified by high-throughput screening, a representative compound was selected and aliovalent substitution was performed to change the Li content in the compound. For each compound, the average Li occupancy, i.e., the ratio between the number of Li ions and the total number of predicted Li sites, was set to the range of 0.5–0.8. One or several dopants were selected and tested according to the substitution probability.^[66] The phase stability for all doped compositions was calculated and the compounds with poor stability were rejected, which have energy above the hull E_{hull} of >50 meV per atom.

For initial diffusional screening, AIMD simulations were performed at two temperatures 1150 and 900 K to screen doped compounds with good phase stability. The materials were excluded with $\sigma_{1150\text{K}} < 33 \text{ mS cm}^{-1}$, which would not likely to be super-ionic at RT and would have large errors in estimating ionic conductivity from AIMD simulations.^[65] The ionic conductivity follows an Arrhenius relationship

$$\sigma T = \sigma_0 \exp\left(-\frac{E_a}{k_B T}\right) \quad (1)$$

where σ is conductivity, T is temperature, σ_0 is the pre-exponential factor, E_a is activation energy, and k_B is the Boltzmann constant. For a material to have $\sigma_{300\text{K}} > 0.1 \text{ mS cm}^{-1}$, the criterion, $1.1 \log(\sigma T)_{1150\text{K}} < \log(\sigma T)_{900\text{K}} - 0.16$, should be satisfied, where σ is in unit of mS cm^{-1} and T is in unit of K. The materials that pass this AIMD screening were further studied in AIMD simulations at five temperatures.

Topological Analysis of Crystal Structural Framework: In order to quantify the features of the crystal structural framework and to predict Li sites, topological analysis of the crystal structural framework was performed

using the Voronoi–Dirichlet partition algorithm implemented in Zeo++.^[67,68] The analysis was performed on the non-Li crystal structural framework generated by removing all Li ions in the structure and used the crystal ionic radius for all ion species.^[69] For sites with partial occupancies of multiple cations, the ion species with the smallest crystal ionic radius were used. For example, the site shared by Ge⁴⁺ and P⁵⁺ in LGPS was treated as P⁵. The Voronoi–Dirichlet partition was performed on the non-Li structural framework. According to the algorithm of Voronoi–Dirichlet partition, the non-Li structural framework was decomposed into multiple Voronoi–Dirichlet polyhedrons, where centers of the polyhedron were ions of the non-Li structural framework.^[67,70,71] Any point within the region of the polyhedron is closer to the center ion than any other ions. The Voronoi node is the vertices shared by the polyhedrons and physically corresponds the center of local void space that may occupy a sphere with the maximal radius r , i.e., the size of Voronoi node.

Topological Analysis of Crystal Structural Framework—Li Node: Each Voronoi node was further screened to remove those with chemical environments that were unsuitable for accommodating Li ions similar to previous studies.^[30–32] Any Voronoi node that was too close to other non-Li cations within the cutoff distance of 2.3 and 2.5 Å for oxides and sulfides, respectively, was removed, while Xiao et al. used a Coulomb repulsion interaction for similar screening.^[31] These values of the cutoff distance were determined by analyzing Li-containing oxide and sulfide compounds, as shown in Figure S1 in the Supporting Information. In addition, the bond valence was calculated for every Voronoi node and the Voronoi nodes with poor values of bond valence were considered unsuitable for Li-ion occupancy and were removed. While Avdeev et al. employed bond-valence mismatch for such purpose,^[32] a cutoff range of bond valence was set for potential Li sites as 0.5–1.2 for oxides and 0.4–1.1 for sulfides, which were chosen to reproduce known experimental Li sites in Li₂O and Li₂S (Figures S2–S6, Supporting Information). Voronoi node that meets these chemical considerations is called “Li node.” In this study, Li node was used as a quantitative description and measure of local space for accommodating Li ions in a crystal structural framework (Section 2.2).

Topological Analysis of Crystal Structural Framework—Li Site: In the topological analysis, Li sites were predicted from groups of Li nodes (Figure 3). The Li nodes were grouped if their corresponding spherical spaces overlapped with each other. The position of a predicted Li site was set as the geometrical center of the group of Li nodes, if the maximum value of d_{ij} , the distance between any two nodes i and j , was smaller than 1.8 Å. If the distance between any two nodes was larger than 1.8 Å, the largest nodes that were separated by a distance of >1.8 Å were selected as the predicted Li site. To measure the total local space of the Li site, the size of a Li site was defined as the value of $r_i + r_j + d_{ij}$, where d_{ij} is the maximum distance between node i and node j among all possible pairs of nodes within the predicted site, and where r_i and r_j are the radius of node i and j , respectively. The size of a Li site is an approximate measure of the total local space of a Li site, and some sites with a large size of >2.2 Å are classified as “enlarged Li sites,” which is a new feature not considered in previous studies.^[30–32] As shown in Section 2.2, the predicted Li sites are in excellent agreement with the experimental Li sites (Figure 3e,f), suggesting the validity of the topological analysis in identifying existing and new Li sites.

Topological Analysis of Crystal Structural Framework—Diffusion Channel and Network: The ion diffusion channels were constructed by connecting Li nodes. The connection of Li nodes better represents the diffusion channels compared to the connection of Li sites because Li nodes directly correspond to local space for Li ion occupancy (Section 2.2). These diffusion channels are in good agreement with Li⁺ trajectories from AIMD simulations (Figure 3). To quantify the connectivity of a 3D Li-ion diffusion network, the minimum node–node distance d that connects Li nodes to form a 3D percolated network was determined. A smaller value of d indicates that smaller distances are required to connect nodes to form a 3D network, and so represents better 3D connectivity of the Li⁺ diffusion network.

Supporting Information

Supporting Information is available from the Wiley Online Library or from the author.

Acknowledgements

X.H. and Q.B. contributed equally to this work. Y.M. acknowledges the computational facilities from the University of Maryland supercomputing resources, the Maryland Advanced Research Computing Center (MARCC). Y.M. acknowledges the financial support from National Science Foundation under Award No. 1550423 for making the code available. The code used for the topological analysis of crystal structures is available in the GitHub repository at https://github.com/mogroupumd/Topological_Analysis.

Conflict of Interest

The authors declare no conflict of interest.

Keywords

ab initio molecular dynamics simulations, computational materials discovery, high-throughput computation, Li-ion conductors, super-ionic conductors

Received: June 27, 2019
Revised: September 21, 2019
Published online:

- [1] B. Dunn, H. Kamath, J.-M. Tarascon, *Science* **2011**, 334, 928.
- [2] J. Janek, W. G. Zeier, *Nat. Energy* **2016**, 500, 300.
- [3] J. Sunarso, S. Baumann, J. M. Serra, W. A. Meulenberg, S. Liu, Y. S. Lin, J. C. D. Da Costa, *J. Membr. Sci.* **2008**, 320, 13.
- [4] E. D. Wachsman, K. T. Lee, *Science* **2011**, 334, 935.
- [5] T. Xu, *J. Membr. Sci.* **2005**, 263, 1.
- [6] K. H. Park, Q. Bai, D. H. Kim, D. Y. Oh, Y. Zhu, Y. Mo, Y. S. Jung, *Adv. Energy Mater.* **2018**, 8, 1800035.
- [7] A. M. Nolan, Y. Zhu, X. He, Q. Bai, Y. Mo, *Joule* **2018**, 2, 2016.
- [8] Y. Seino, T. Ota, K. Takada, A. Hayashi, M. Tatsumisago, *Energy Environ. Sci.* **2014**, 7, 627.
- [9] Y. Kato, S. Hori, T. Saito, K. Suzuki, M. Hirayama, A. Mitsui, M. Yonemura, H. Iba, R. Kanno, *Nat. Energy* **2016**, 1, 16030.
- [10] Y. Wang, W. D. Richards, S. P. Ong, L. J. Miara, J. C. Kim, Y. Mo, G. Ceder, *Nat. Mater.* **2015**, 14, 1026.
- [11] Y. S. Jung, D. Y. Oh, Y. J. Nam, K. H. Park, *Isr. J. Chem.* **2015**, 55, 472.
- [12] N. Kamaya, K. Homma, Y. Yamakawa, M. Hirayama, R. Kanno, M. Yonemura, T. Kamiyama, Y. Kato, S. Hama, K. Kawamoto, A. Mitsui, *Nat. Mater.* **2011**, 10, 682.
- [13] V. Thangadurai, H. Kaack, W. J. F. Weppner, *J. Am. Ceram. Soc.* **2003**, 86, 437.
- [14] R. Murugan, V. Thangadurai, W. Weppner, *Angew. Chem., Int. Ed.* **2007**, 46, 7778.
- [15] H. Aono, E. Sugimoto, Y. Sadaoka, N. Imanaka, G. y. Adachi, *J. Electrochem. Soc.* **1990**, 137, 1023.
- [16] K. Arbi, J. M. Rojo, J. Sanz, *J. Eur. Ceram. Soc.* **2007**, 27, 4215.
- [17] A. Manthiram, X. Yu, S. Wang, *Nat. Rev. Mater.* **2017**, 2, 16103.
- [18] G. L. Zhu, C. Z. Zhao, J. Q. Huang, C. He, J. Zhang, S. Chen, L. Xu, H. Yuan, Q. Zhang, *Small* **2019**, 15, 1805389.

- [19] H. Aono, E. Sugimoto, Y. Sadaoka, N. Imanaka, G.-y. Adachi, *Solid State Ionics* **1990**, *40*, 38.
- [20] V. Thangadurai, S. Narayanan, D. Pinzaru, *Chem. Soc. Rev.* **2014**, *43*, 4714.
- [21] S. P. Ong, Y. Mo, W. D. Richards, L. Miara, H. S. Lee, G. Ceder, *Energy Environ. Sci.* **2013**, *6*, 148.
- [22] S. Hull, *Rep. Prog. Phys.* **2004**, *67*, 1233.
- [23] J. C. Bachman, S. Muy, A. Grimaud, H.-H. Chang, N. Pour, S. F. Lux, O. Paschos, F. Maglia, S. Lupart, P. Lamp, L. Giordano, Y. Shao-Horn, *Chem. Rev.* **2015**, *116*, 140.
- [24] X. He, Y. Zhu, Y. Mo, *Nat. Commun.* **2017**, *8*, 15893.
- [25] R. Jalem, Y. Yamamoto, H. Shiiba, M. Nakayama, H. Munakata, T. Kasuga, K. Kanamura, *Chem. Mater.* **2013**, *25*, 425.
- [26] M. Xu, J. Ding, E. Ma, *Appl. Phys. Lett.* **2012**, *101*, 031901.
- [27] B. Kozinsky, S. A. Akhade, P. Hirel, A. Hashibon, C. Elsässer, P. Mehta, A. Logeat, U. Eisele, *Phys. Rev. Lett.* **2016**, *116*, 055901.
- [28] K. E. Kweon, J. B. Varley, P. Shea, N. Adelstein, P. Mehta, T. W. Heo, T. J. Udovic, V. Stavila, B. C. Wood, *Chem. Mater.* **2017**, *29*, 9142.
- [29] Y. Wang, M. Klenk, K. Page, W. Lai, *Chem. Mater.* **2014**, *26*, 5613.
- [30] N. A. Anurova, V. A. Blatov, *Acta Crystallogr., Sect. B: Struct. Sci.* **2009**, *65*, 426.
- [31] R. Xiao, H. Li, L. Chen, *J. Materiomics* **2015**, *1*, 325.
- [32] M. Avdeev, M. Sale, S. Adams, R. P. Rao, *Solid State Ionics* **2012**, *225*, 43.
- [33] M. Monchak, T. Hupfer, A. Senyshyn, H. Boysen, D. Chernyshov, T. Hansen, K. G. Schell, E. C. Bucharsky, M. J. Hoffmann, H. Ehrenberg, *Inorg. Chem.* **2016**, *55*, 2941.
- [34] D. A. Weber, A. Senyshyn, K. S. Weldert, S. Wenzel, W. Zhang, R. Kaiser, S. Berendts, J. Janek, W. G. Zeier, *Chem. Mater.* **2016**, *28*, 5905.
- [35] Y. Wang, A. Huq, W. Lai, *Solid State Ionics* **2014**, *255*, 39.
- [36] O. Kwon, M. Hirayama, K. Suzuki, Y. Kato, T. Saito, M. Yonemura, T. Kamiyama, R. Kanno, *J. Mater. Chem. A* **2015**, *3*, 438.
- [37] S. Hori, S. Taminato, K. Suzuki, M. Hirayama, Y. Kato, R. Kanno, *Acta Crystallogr., Sect. B: Struct. Sci., Cryst. Eng. Mater.* **2015**, *71*, 727.
- [38] A. Kuhn, J. Köhler, B. V. Lotsch, *Phys. Chem. Chem. Phys.* **2013**, *15*, 11620.
- [39] A. Jain, G. Hautier, S. P. Ong, C. J. Moore, C. C. Fischer, K. A. Persson, G. Ceder, *Phys. Rev. B* **2011**, *84*, 045115.
- [40] H. Xie, J. A. Alonso, Y. Li, M. T. Fernández-Díaz, J. B. Goodenough, *Chem. Mater.* **2011**, *23*, 3587.
- [41] R. P. Rao, W. Gu, N. Sharma, V. K. Peterson, M. Avdeev, S. Adams, *Chem. Mater.* **2015**, *27*, 2903.
- [42] K. Kataoka, H. Nagata, J. Akimoto, *Sci. Rep.* **2018**, *8*, 9965.
- [43] G. Bergerhoff, R. Hundt, R. Sievers, I. D. Brown, *J. Chem. Inf. Model.* **1983**, *23*, 66.
- [44] H.-P. Hong, *Mater. Res. Bull.* **1978**, *13*, 117.
- [45] K. Toda, S. Kurita, M. Sato, *J. Ceram. Soc. Jpn.* **1996**, *104*, 140.
- [46] H. Yamane, M. Shibata, Y. Shimane, T. Junke, Y. Seino, S. Adams, K. Minami, A. Hayashi, M. Tatsumisago, *Solid State Ionics* **2007**, *178*, 1163.
- [47] Z. Liu, W. Fu, E. A. Payzant, X. Yu, Z. Wu, N. J. Dudney, J. Kiggans, K. Hong, A. J. Rondinone, C. Liang, *J. Am. Chem. Soc.* **2013**, *135*, 975.
- [48] W. D. Richards, Y. Wang, L. J. Miara, J. C. Kim, G. Ceder, *Energy Environ. Sci.* **2016**, *9*, 3272.
- [49] T. Suzuki, K. Yoshida, K. Uematsu, T. Kodama, K. Toda, Z.-G. Ye, M. Ohashi, M. Sato, *Solid State Ionics* **1998**, *113*, 89.
- [50] A. Bykov, A. Chirkin, L. Demyanets, S. Doronin, E. Genkina, A. Ivanov-Shits, I. Kondratyuk, B. Maksimov, O. Mel'Nikov, L. Muradyan, *Solid State Ionics* **1990**, *38*, 31.
- [51] M. T. Chowdhury, R. Takekawa, Y. Iwai, N. Kuwata, J. Kawamura, *J. Chem. Phys.* **2014**, *140*, 124509.
- [52] S. Boulineau, M. Courty, J.-M. Tarascon, V. Viallet, *Solid State Ionics* **2012**, *221*, 1.
- [53] A. Emly, E. Kioupakis, A. Van der Ven, *Chem. Mater.* **2013**, *25*, 4663.
- [54] Z. Zhu, I.-H. Chu, S. P. Ong, *Chem. Mater.* **2017**, *29*, 2474.
- [55] X. He, Y. Mo, *Phys. Chem. Chem. Phys.* **2015**, *17*, 18035.
- [56] S. Duluard, A. Paillassa, L. Puech, P. Vinatier, V. Turq, P. Rozier, P. Lenormand, P.-L. Taberna, P. Simon, F. Ansart, *J. Eur. Ceram. Soc.* **2013**, *33*, 1145.
- [57] M. A. Kraft, S. P. Culver, M. Calderon, F. Böcher, T. Krauskopf, A. Senyshyn, C. Dietrich, A. Zevalkink, J. r. Janek, W. G. Zeier, *J. Am. Chem. Soc.* **2017**, *139*, 10909.
- [58] A. Düvel, P. Heitjans, P. Fedorov, G. Scholz, G. Cibin, A. V. Chadwick, D. M. Pickup, S. Ramos, L. W. L. Sayle, E. K. L. Sayle, *J. Am. Chem. Soc.* **2017**, *139*, 5842.
- [59] D. Di Stefano, A. Miglio, K. Robeyns, Y. Filinchuk, M. Lechartier, A. Senyshyn, H. Ishida, S. Spannenberger, D. Prutsch, S. Lünghammer, *Chem* **2019**, *5*, 2450.
- [60] G. Kresse, J. Furthmüller, *Phys. Rev. B* **1996**, *54*, 11169.
- [61] J. P. Perdew, M. Ernzerhof, K. Burke, *J. Chem. Phys.* **1996**, *105*, 9982.
- [62] A. Jain, G. Hautier, C. J. Moore, S. Ping Ong, C. C. Fischer, T. Mueller, K. A. Persson, G. Ceder, *Comput. Mater. Sci.* **2011**, *50*, 2295.
- [63] A. Jain, S. P. Ong, G. Hautier, W. Chen, W. D. Richards, S. Dacek, S. Cholia, D. Gunter, D. Skinner, G. Ceder, K. A. Persson, *APL Mater.* **2013**, *1*, 011002.
- [64] S. Nose, *Prog. Theor. Phys. Suppl.* **1991**, *103*, 1.
- [65] X. He, Y. Zhu, A. Epstein, Y. Mo, *npj Comput. Mater.* **2018**, *4*, 18.
- [66] G. Hautier, C. Fischer, V. Ehrlicher, A. Jain, G. Ceder, *Inorg. Chem.* **2010**, *50*, 656.
- [67] T. F. Willems, C. H. Rycroft, M. Kazi, J. C. Meza, M. Haranczyk, *Microporous Mesoporous Mater.* **2012**, *149*, 134.
- [68] R. L. Martin, B. Smit, M. Haranczyk, *J. Chem. Inf. Model.* **2012**, *52*, 308.
- [69] R. D. Shannon, *Acta Crystallogr., Sect. A: Cryst. Phys., Diffr., Theor. Gen. Crystallogr.* **1976**, *32*, 751.
- [70] R. L. Martin, B. Smit, M. Haranczyk, *J. Chem. Inf. Model.* **2011**, *52*, 308.
- [71] V. A. Blatov, A. P. Shevchenko, V. N. Serenzhkin, *Acta Crystallogr., Sect. A: Found. Crystallogr.* **1995**, *51*, 909.